Resonant soft x-ray scattering investigation of orbital and magnetic ordering in $La_{0.5}Sr_{1.5}MnO_4$

S. B. Wilkins,[1,2] N. Stojić,[3] T. A. W. Beale,[4] N. Binggeli,[3] C. W. M. Castleton,[5,6] P. Bencok,[2] D. Prabhakaran,[7] A. T. Boothroyd,[7] P. D. Hatton,[4] and M. Altarelli[3,8]

[1]*European Commission, Joint Research Center, Institute for Transuranium Elements, Hermann von Helmholtz-Platz 1, 76344 Eggenstein-Leopoldshafen, Germany*

[2]*European Synchrotron Radiation Facility, Boîte Postal 220, F-38043 Grenoble Cedex, France*

[3]*Abdus Salam International Centre for Theoretical Physics, Trieste 34014, Italy*

[4]*Department of Physics, University of Durham, Rochester Building, South Road, Durham, DH1 3LE, United Kingdom*

[5]*Materials and Semiconductor Physics Laboratory, Royal Institute of Technology (KTH), Electrum 229, 16440 Kista, Sweden*

[6]*Department of Physical Electronics/Photonics, ITM, Mid Sweden University, 85170 Sundsvall, Sweden*

[7]*Department of Physics, University of Oxford, Clarendon Laboratory, Parks Road, Oxford, OX1 3PU, United Kingdom*

[8]*Sincrotrone Trieste, Area Science Park, 34012 Basovizza, Trieste, Italy*

(Received 27 October 2004; revised manuscript received 12 January 2005; published 3 June 2005)

We report resonant x-ray scattering data of the orbital and magnetic ordering at low temperatures at the Mn $L_{2,3}$ edges in $La_{0.5}Sr_{1.5}MnO_4$. The orderings display complex energy features close to the Mn absorption edges. Systematic modeling with atomic multiplet crystal field calculations was used to extract meaningful information regarding the interplay of spin, orbital, and Jahn-Teller order. These calculations provide a good general agreement with the observed energy dependence of the scattered intensity for a dominant orbital ordering of the $d_{x^2-z^2}/d_{y^2-z^2}$ type. In addition, the origins of various spectral features are identified. The temperature dependence of the orbital and magnetic ordering was measured and suggests a strong interplay between the magnetic and orbital order parameters.

DOI: 10.1103/PhysRevB.71.245102 PACS number(s): 71.30.+h, 61.10.−i, 75.25.+z, 75.47.Lx

I. INTRODUCTION

Orbital ordering, which involves correlations between the spatial distribution of the outermost valence electrons, has long been considered a vital ingredient in the structural and physical properties of strongly correlated electron systems such as transition metal oxides. The competition and cooperation between the charge, orbital, and spin degrees of freedom of the electrons manifest themselves in in unusual properties such as high temperature superconductivity, colossal magnetoresistance, and magnetostructural transitions.[1] In particular, charge-orbital ordering in half-doped manganites has attracted much attention and controversy.[2–6] In $La_{0.5}Sr_{1.5}MnO_4$ the Mn sites are all crystallographically equivalent at room temperature with an average valency of 3.5. This material displays a phase transition at ~240 K below which it was believed that charge disproportionation of the Mn ions occurs,[7,8] creating two inequivalent sites identified as Mn^{3+} and Mn^{4+}. This was originally predicted by Goodenough.[9] It should be noted that the picture of integral charge on the Mn ions has recently been challenged,[10] implying that the actual valence difference of the two Mn ions is much less than 1. The assumption that they are close to 3.5+, however, is based on the formal valence and does not take covalency into account, which should cause a reduction; according to Hartree-Fock calculations on the related compound $La_{0.5}Ca_{0.5}MnO_3$ (Ref. 11), the charge on the manganese ion is even below 3+. In this paper, we adopt a multiplet picture which applies to integer charge only and we assume the value of 3+ as the closest to the real situation. The strong Hund's rule coupling and the cubic (O_h) component of the crystal field implies that the Mn^{3+} $3d^4$ site has three electrons in the $t_{2g\uparrow}$ level and one electron in the twofold degenerate $e_{g\uparrow}$ level. The degeneracy of the $e_{g\uparrow}$ level can be lifted by cooperative Jahn-Teller distortions of the MnO_6 octahedra reducing the symmetry to D_{4h}. Adding the tetragonal field, the $t_{2g\uparrow}$ level splits into d_{xy} and doubly-degenerate $d_{xz,yz}$ orbitals, while the $e_{g\uparrow}$ level splits into $d_{3z^2-r^2}$ and $d_{x^2-y^2}$. Therefore, depending on the value of the applied tetragonal crystal field, Mn^{3+} will have as a ground state filled $t_{2g\uparrow}$ levels and the $e_{g\uparrow}$ orbital lying along the elongation direction, either a $d_{3z^2-r^2}$ or a $d_{x^2-y^2}$ orbital [see Figs. 1(a) and 1(b), respectively], which will determine the type of the orbital ordering. Further cooling below $T_N \sim 120$ K results in long range antiferromagnetic ordering of manganese ions into a CE-type structure.[12] This was the basis of an alternative model put forward by Goodenough[9] in which orbital order correlations lower the energy by favoring antiferromagnetic interactions. Until very recently, detailed investigations of the origin of the orbital order remained elusive because of the lack of a technique capable of direct observation.

Resonant x-ray scattering (RXS) studies of $La_{0.5}Sr_{1.5}MnO_4$ were first attempted at the manganese K edge. The diffraction intensity at an orbital ordering reflection displayed a striking resonant enhancement near the absorption edge and a specific dependence on the azimuthal angle.[13] There are two possible mechanisms[14] for obtaining resonant enhancement at an orbital-ordering Bragg vector: Jahn-Teller distortions and orbital ordering. Cooperative Jahn-Teller distortions originate from a bare structural origin, i.e., a periodic distortion of the oxygen octahedra. Orbital ordering is related to the occupation of different $e_{g\uparrow}$ orbitals. The Mn K edge resonance, which involves virtual excitations from 1s to 4p bands, is generally insensitive to orbital order-

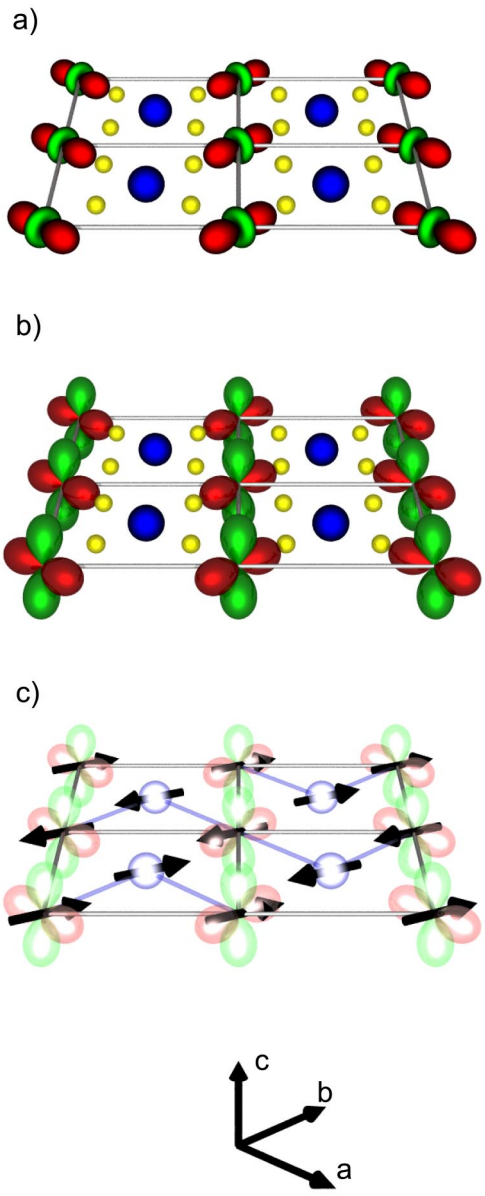

FIG. 1. (Color online) The structure of $La_{0.5}Sr_{1.5}MnO_4$. (a) and (b) show two different types of orbital ordering, $d_{3x^2-r^2}/d_{3y^2-r^2}$ type in (a) and $d_{x^2-z^2}/d_{y^2-z^2}$ in (b). (c) shows the magnetic ordering with blue lines representing the ferromagnetic spin chains. The orbitals are drawn for the Mn^{3+} ions, while the small yellow circles represent oxygen atoms and large blue circles represent the Mn^{4+} ions.

ing of the 3*d* states. Theoretical studies proposed that the observed sensitivity is largely due to Jahn-Teller distortions via 4*p* band structure effects,[15–20] rather than to 3*d* orbital ordering via 3*d*–4*p* Coulomb interactions.[21] This conclusion was recently supported by experimental work on strained manganite films.[22] Experiments performed at the *L* edges, on the other hand, directly probe the 3*d* states. Resonant soft x-ray diffraction at the Mn *L* edges was first reported by Wilkins *et al.*[23] and was followed by the first direct observations of orbital ordering using soft x rays in $La_{0.5}Sr_{1.5}MnO_4$.[24] Aided by earlier theoretical predictions[25] they reported energy resonances at the Mn L_3 and L_2 edges, proposing that the orbital ordering was caused by a mixture of both cooperative Jahn-Teller distortions and direct Goodenough orbital correlations. Similar experimental results were later independently reported by another group.[26] More recently, the same technique has been used to study magnetic and orbital correlations in $Pr_{0.6}Ca_{0.4}MnO_3$.[27]

In this paper, we present a combined experimental and theoretical study of both magnetic and orbital order reflection spectra at low temperatures in $La_{0.5}Sr_{1.5}MnO_4$. The analysis of the spectra is based on atomic multiplet calculations incorporating crystal field effects. We present the spectra obtained by fitting the crystal field parameters and discuss their agreement with the experimental spectra. Further, we indicate the dominant orbital ordering type. We also present analysis of the superlattice reflections in terms of the Jahn-Teller versus orbital ordering origin of the spectral features. Finally, we have measured the temperature dependence of certain features in the energy resonant spectrum. These show a dramatic change at a temperature corresponding to the Néel temperature, indicative of a strong interplay between the magnetic and orbital order parameters.

This paper is organized as follows: Section II of the paper describes the methods to obtain the spectra, experimental and theoretical. The results are presented in Sec. III, where experimental spectra and theoretical fits are compared. There we also present the analysis of the Jahn-Teller contributions to the orbital ordering scattering. Section IV describes the temperature dependence of the spectra, while all our results are summarized in the conclusions in Sec. V.

II. METHOD

A. Experimental approach

The experiments were performed at beamlines 5U1 at Daresbury and ID08 at the European Synchrotron Radiation Facility (ESRF). Single crystals of $La_{0.5}Sr_{1.5}MnO_4$ with dimensions $10\times3\times3$ mm^3 were grown at the University of Oxford using the floating zone method. They were cut with either [110] or $[1\bar{1}2]$ directions surface normal and polished with 0.25 μm diamond paste to a flat shiny surface.

The crystals were mounted in the ID08 five-circle diffractometer operating at a base pressure of 1×10^{-8} mbar, and equipped with a Si diode detector. The beamline produces ~100% linearly polarized x rays. At ~650 eV an energy resolution of 165 meV was obtained. Sample cooling was achieved using a liquid He cryostat attached to the sample stage by copper braids resulting in a base temperature of 63 K.

On the 5U1 beamline, crystals were mounted on a two circle diffractometer enclosed in a high vacuum chamber with a base pressure of 1×10^{-8} mbar. The incident beam has a resolution of 500 meV, and a beam size of 1×1 mm^2. The sample was mounted on a liquid nitrogen cooled copper block, with a small manual χ adjustment for initial orientation. The base temperature achieved was 83 K. Temperature stability between 83 K and 300 K was achieved with a heater element, and control thermometer mounted next to the sample.

TABLE I. The Hartree-Fock values for the ground and excited states of Mn^{3+} given in eV. Coulomb and exchange integrals in the calculation have been scaled to 75% of their atomic values. The *p*-shell spin-orbit parameter $\zeta(2p)$ has been increased by 9% from the Hartree-Fock value to correspond to the experimental value (Ref. 33).

	$F^2(d,d)$	$F^4(d,d)$	$F^2(p,d)$	$G^1(p,d)$	$G^3(p,d)$	$\zeta(2p)$	$\zeta(3d)$
$3d^4$	11.415	7.148	⋯	⋯	⋯	⋯	0.046
$2p^5 3d^5$	12.210	7.649	6.988	5.179	2.945	7.467	0.059

At both beamlines the experimental procedure was identical. The incident energy was set to the manganese L_3 edge, and superlattice peaks located at the $(\frac{1}{4},\frac{1}{4},0)$ and $(\frac{1}{4},-\frac{1}{4},\frac{1}{2})$ positions. Each reflection was measured on a separate sample. Energy scans of the reflections were performed at fixed wave vector with the incident polarization perpendicular to the scattering plane (σ polarization). No analysis of the polarization of the scattered x rays was performed. The integrated intensity was measured by longitudinal scans through the peak at fixed energy.

The azimuthal dependence of the orbital order superlattice reflection was measured on the ID08 diffractometer by rotating the sample around the scattering vector, $\vec{q}$. In the absence of an orientation matrix (UB) this was achieved by rotation of the diffractometer's ϕ axis. The origin of the azimuthal angle Ψ corresponds to the situation where the [001] direction lies within the scattering plane.

B. Theoretical model

The calculations of the RXS spectra are based on atomic multiplet calculations in a crystal field. The calculations were performed at 0 K. Cowan's atomic multiplet program[28–30] provides *ab initio* (Hartree-Fock) values of the radial Coulomb (Slater) integrals $F^{0,2,4}(d,d)$, $F^2(p,d)$, $G^{1,3}(p,d)$ (direct and exchange contributions) and the spin-orbit interactions $\zeta(2p)$ and $\zeta(3d)$ for an isolated Mn^{3+} ion. Their values are given in Table I. As we are lowering the symmetry by the inclusion of the crystal field, we apply the Wigner-Eckart theorem to calculate matrix elements in a given point group[31] starting from the matrix elements evaluated in the spherical group. This is implemented in the "Racah" code, which also gives the values of the dipole transition matrix elements, necessary for the calculation of the spectra, as will be described in the following subsection. The fitting procedure starts with adjusting the crystal field type and strength by modifying the cubic (X^{400}) and tetragonal (X^{220}) crystal field parameters. Orbital and magnetic spectra calculated using the atomic multiplet code and including the crystal field effects are then compared to the experimental data and the procedure is continued until the optimized set of crystal field parameters is found. In order to take into account the screening effects present in a real crystal with respect to the atomic picture, we scale down all the Slater integrals to 75% of their atomic values.

In the actual $La_{0.5}Sr_{1.5}MnO_4$ compound, the spins are approximately aligned in the [110] direction,[32] displaying antiferromagnetic ordering along the *c* axis and between the spin chains, and ferromagnetic along the spin chains, as shown in Fig. 1(c). In order to simulate the effects of the spin ordering on an isolated ion (superexchange and direct exchange interactions), we introduce a magnetic field acting on the spin of the atom. This field splits additionally the $S=2$ quintet into $S_z=-2,-1,\ldots,2$ levels. Inclusion of the magnetic field favors the $S_z=-2$ level as the ground state of the atom. The strength of the exchange interaction was set to 0.02 eV.

Using the above procedure one readily obtains the eigenvalues for the ground ($3d^n$) and excited ($2p^5 3d^{n+1}$) states separately. The next step towards the calculation of the scattering or absorption spectrum is the evaluation of the dipole transition probability. Depending on the crystal symmetry and the type of scattering one is interested in, the angular dependence and the matrix elements value of the transition operators of the resonant amplitude will vary.[34]

The crystal field has the tetragonal (D_{4h}) symmetry. However, if the spin direction is assumed along [110], the site symmetry is lowered to that of the C_i point group. We note that the spin direction has a non-negligible influence on the RXS spectra. In most of the previous studies (for example, in Ref. 25), the spin was aligned along the highest symmetry direction of the local crystal field (fourfold axis). This gives rise to an artificial 90° spin-canted structure and to spectra which differ significantly from the ones obtained using collinear spins. In the present work, following the approach described by Carra and Thole,[34] we derived the expression which describes the atomic resonant scattering amplitude in the C_i point group[35] and, taking into account the structure factor, computed the orbital and magnetic scattering intensity. In the case of the orbital scattering with the wave vector $(\frac{1}{4},\frac{1}{4},0)$, the resonant scattering intensity is proportional to the following combination of the atomic scattering tensor components:

$$I_{\mathrm{res}}^{\mathrm{OO}} \propto |F_{0;1}^{\mathrm{e}} - F_{0;-1}^{\mathrm{e}} + F_{1;0}^{\mathrm{e}} - F_{-1;0}^{\mathrm{e}}|^2, \tag{1}$$

with $F_{m;m'}^{\mathrm{e}}$ defined as

$$F_{\mathrm{m;m'}}^{\mathrm{e}} = \sum_n \frac{\langle 0|J_{\mathrm{m}}^{1\dagger}|n\rangle\langle n|J_{\mathrm{m'}}^{1}|0\rangle}{E_0 - E_n + \hbar\omega + i\Gamma/2}, \tag{2}$$

where m and m' denote polarization states and J_m^1 are the electric dipole operators defined in spherical coordinates. $|0\rangle$ represents the ground state with energy E_0 and $|n\rangle$ intermediate state with energy E_n. The photon energy is $\hbar\omega$ and Γ stands for the broadening due to the core-hole lifetime.

Similarly, for the magnetic scattering with the wave vector $(\frac{1}{4},-\frac{1}{4},\frac{1}{2})$, the scattering intensity can be expressed as

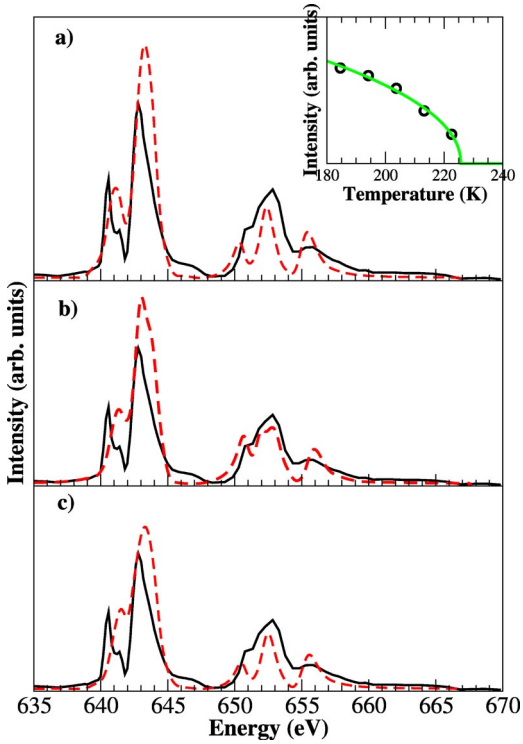

FIG. 2. (Color online) The energy scan through the $(\frac{1}{4},\frac{1}{4},0)$ orbital order reflection at constant wave vector at 63 K (full black line) with the theoretical fits (dashed red lines) for the (a) $d_{x^2-z^2}$ and (b) $d_{3x^2-r^2}$ types of orbital ordering. In the panel (c) we present the fit for the orthorhombic crystal field. Shown in the inset is the temperature evolution of the orbital order parameter.

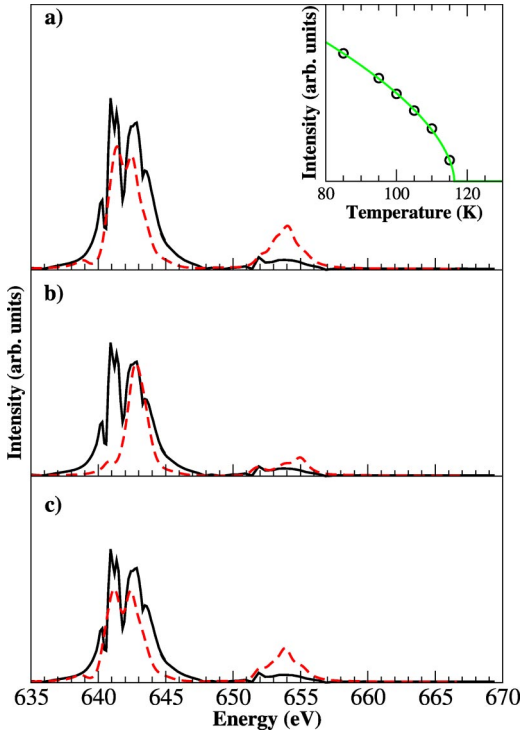

FIG. 3. (Color online) The energy scan through the $(\frac{1}{4},-\frac{1}{4},\frac{1}{2})$ magnetic order reflection at constant wave vector at 63 K (full black line) with the theoretical fits (dashed red lines) for the (a) $d_{x^2-z^2}$ and (b) $d_{3x^2-r^2}$ types of orbital ordering. In the panel (c) we present the fit for the orthorhombic crystal field. The inset shows the temperature evolution of the magnetic order parameter.

$$I_{\mathrm{res}}^{\mathrm{MO}} \propto |F_{1;1}^{\mathrm{e}} - F_{-1;-1}^{\mathrm{e}}|^2, \tag{3}$$

which is identical to the expression derived for the spherical symmetry.[36] We note that the proportionality coefficients that contain the polarization dependence are omitted from Eqs. (1) and (3).

In these calculations we used $\Gamma = 0.5$ eV and, in addition, the scattering intensity was convoluted with a Gaussian of width 0.1 eV to simulate the experimental (energy) resolution.

III. ORBITAL AND MAGNETIC SCATTERING

Figure 2 shows the energy dependence of the scattered intensity at a fixed wave vector of $\vec{q}_{OO}=(\frac{1}{4},\frac{1}{4},0)$ through the Mn L_3 and L_2 edges. This wave vector corresponds to the long range orbital ordering of the Mn^{3+} ions within the *a*-*b* plane. These data were collected at the beamline ID08 on a single crystal cut with the [110] direction surface normal. On initial inspection, the spectrum is dominated by scattering at the L_3 edge where two distinct features are present. The scattering is weaker at the L_2 edge where three convoluted peaks are observed. Figure 3 shows the energy dependence collected in a similar fashion, but at a wave vector of $\vec{q}_{AF}=(\frac{1}{4},-\frac{1}{4},\frac{1}{2})$. This reflection corresponds to long range antiferromagnetic ordering on the Mn^{3+} sublattice. The observation of a *c*-axis component in the wave vector of the antiferromagnetic reflection (compared to the orbital order wave vector) indicates that while the orbitals are ferro-ordered along the [001] direction, the magnetic moments are aligned antiferromagnetically. The magnetic ordering energy spectra is even more dominated by scattering at the L_3 edge, which is observed to contain up to five separate features. The L_2 features are much weaker and contain only two main peaks. These data show no relative shift in energy between magnetic and orbital spectra, at variance to what was reported by Thomas *et al.*[27] The insets of Figs. 2 and 3 show the temperature evolution of the orbital and magnetic order parameters, respectively. The orbital order parameter was found to decrease in a continuous fashion with increasing temperature in the vicinity of $T_{OO}=230$ K. The antiferromagnetic reflection shows the same behavior, albeit, with the lower transition temperature of $T_N=120$ K.

Figure 4 displays the integrated intensity of the orbital order superlattice reflection as a function of the azimuthal angle Ψ. The solid line shows a simulation of the azimuthal dependence given by the following equation,

$$I(\theta,\psi) \propto \cos^2\theta_B \cos^2\Psi \cdot I_{\mathrm{res}}^{OO}, \tag{4}$$

where θ_B is the Bragg angle of the reflection and ψ is the azimuthal angle. This dependence is characteristic of the $E1$ resonant scattering process. It is worth mentioning that this azimuthal dependence, which shows an extinction of the scattering when $\Psi \approx 90°$, is not consistent with scattering

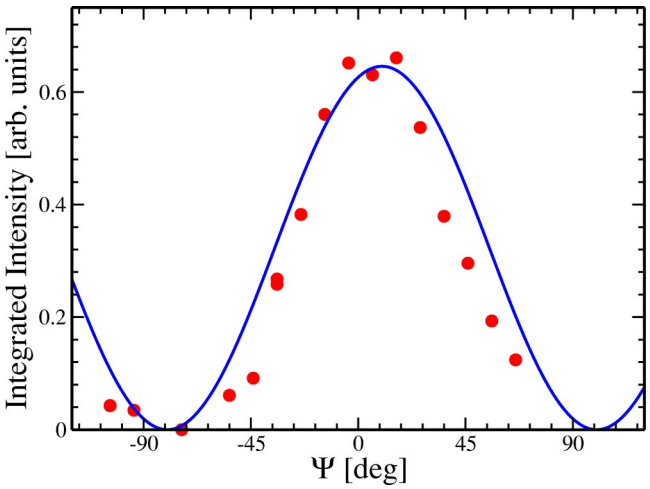

FIG. 4. (Color online) The dependence of the integrated intensity as a function of azimuthal angle Ψ for the $(\frac{1}{4},\frac{1}{4},0)$ superlattice reflection at 63 K (circles). The solid line is a simulation of the azimuthal dependence for the proposed orbital order.

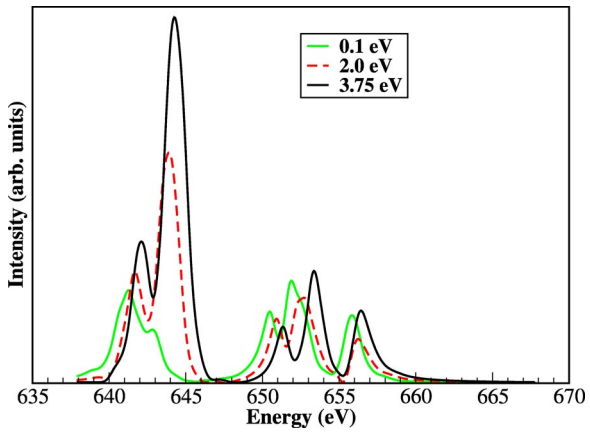

FIG. 5. (Color online) The variation of the Jahn-Teller effect through the reduction of the tetragonal crystal field: $X^{220}=3.75$ eV (full black line), 2 eV (dashed red line), and 0.1 eV (full green line).

from the magnetic structure with moments aligned along [210]. Therefore we conclude that the scattering observed at the $(\frac{1}{4},\frac{1}{4},0)$ position arises solely from the orbital ordering.

In Fig. 2(a) we also present the best fit we have obtained for the orbital scattering by fitting simultaneously both the magnetic and orbital scattering to the same crystal field parameters. The fitting procedure yielded the following optimized crystal field parameters: $X^{400}=5.6$ eV and $X^{220}=3.75$ eV, or $10D_q=1.70$ eV and $D_s=-0.45$ eV. The same field can be expressed in terms of the energy of the $3d$ orbitals:[37] $E(d_{xy})=-1.58$ eV, $E(d_{xz,yz})=-0.23$ eV, $E(d_{x^2-z^2})=-0.12$ eV, and $E(d_{3x^2-r^2})=1.92$ eV. This corresponds to orbital ordering of the $d_{x^2-z^2}/d_{y^2-z^2}$ type, as illustrated in Fig 1(b). This is in contrast to the conventional model of orbital ordering of the $d_{3x^2-r^2}/d_{3y^2-r^2}$ type,[15,25,26] or even the partial occupancy alternating $d_{3x^2-r^2}/d_{3y^2-r^2}$ and $d_{x^2-y^2}$ model,[38] but in agreement with the findings of Huang *et al.* in a recent dichroism study on $La_{0.5}Sr_{1.5}MnO_4$.[39] Magnetic scattering corresponding to the same crystal field parameters is shown in Fig. 3(a). All the features of the L_3 and L_2 structures of the orbital scattering fit display good agreement with the experimental data although the L_3/L_2 branching ratio is somewhat overestimated, and the high-energy shoulder of the L_3 peak is not reproduced. The magnetic scattering is also well described, but it overestimates the intensity of the L_2 peak. Both low- and high-energy shoulders in the L_3 peak are not present in the fit.

The fit corresponding to the crystal field described by $X^{400}=5.6$ eV and $X^{220}=-1.65$ eV reproduced the spectrum for the orbital scattering very well, Fig. 2(b), but the magnetic scattering was poorly described, completely missing the first feature in the L_3 peak. We also note that the addition of a small orthorhombic (D_{2h}) component, $X^{222}=-1.1$ eV, to the crystal field related to the $d_{x^2-z^2}/d_{y^2-z^2}$ type of the orbital ordering improved the L_3/L_2 ratio for the orbital and magnetic scattering, as shown in Figs. 2(c) and 3(c).

In order to address the origin of the different spectral features, we have examined the effect of a reduction of the tetragonal part (X^{220}) of the crystal field, using different values of X^{220} as shown in Fig. 5. This approach is based on the fact that changes of the Jahn-Teller distortion yield corresponding changes to the tetragonal field. We conclude that the reduction of the Jahn-Teller effect results in the reduced L_3/L_2 ratio and in the drastic reduction of the main feature at the L_3 edge.

IV. TEMPERATURE DEPENDENCE

The orbital order spectrum shown in Fig. 2 was obtained at a temperature of 63 K. We also made measurements of spectral features in the $(\frac{1}{4},\frac{1}{4},0)$ orbital order reflection as a function of temperature, upon warming, to measure the change of the crystal field. These measurements were performed on station 5U1 and the energy resolution (ΔE) was deliberately reduced to approximately integrate the spectral feature over energy. These results are displayed in Fig. 6.

Figure 5 shows that the scattered intensity at the L_3 edge is very sensitive to the Jahn-Teller effect while the intensity at the L_2 edge is not. We define, for the purposes of this discussion, the branching ratio (Fig. 6, middle panel) as the ratio of integrated intensities (over $\vec{q}$) measured at energies of 643 and 653 eV for the L_3 and L_2 edges, respectively, shown in Fig. 6 (top panel).This branching ratio is expected to give an indication of the Jahn-Teller distortion.

Upon cooling past T_{OO} the branching ratio increases, suggesting an increase in the Jahn-Teller distortion. Approaching T_N the integrated intensity for both spectral features rises sharply. However, the branching ratio also increases at this point, indicating that the Jahn-Teller distortion becomes even more dominant. At T_N, as indicated by the measured magnetic order parameter in the bottom panel of Fig. 6, both the integrated intensity and the branching ratio saturate. Upon further cooling only a slight decrease in the branching ratio is observed.

At temperatures below T_N, the orbital order correlations are approximately constant even as the antiferromagnetic spin correlations are gradually increasing. The dramatic in-

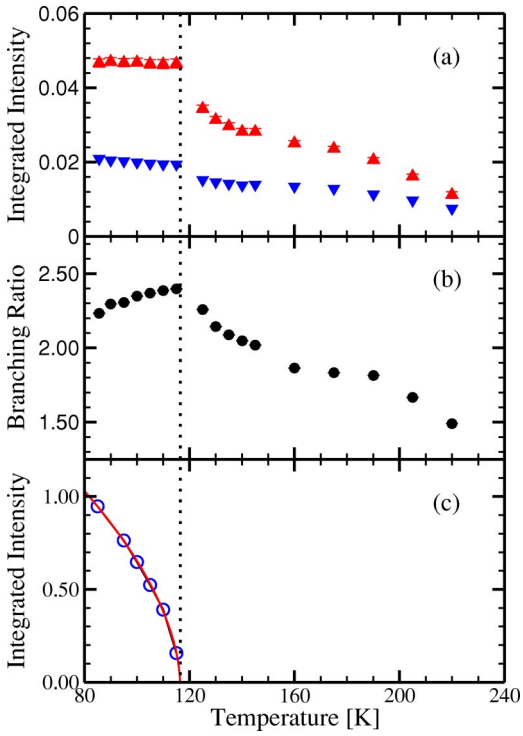

FIG. 6. (Color online) (a) The temperature dependence of the integrated intensity (over $\vec{q}$) of the main features at the L_3 edge (triangles) and at the L_2 edge (inverted triangles). (b) The temperature dependence of the ratio of the integrated intensities L_3/L_2. (c) The temperature dependence of the integrated intensity of the $(\frac{1}{4},-\frac{1}{4},\frac{1}{2})$ magnetic reflection measured at 643 eV.

crease in the intensity of the orbital ordering superlattice reflection at T_N is very unexpected. The stepwise increase in the integrated intensity suggests that the long-range orbital ordering interactions maximize at T_N. The temperature region between T_N and T_{OO} is one in which the orbital order correlations gradually increase with decreasing temperatures. These results suggest a strong interaction between the orbital and spin degrees of freedom. Is such behavior typical, or restricted to just $La_{0.5}Sr_{1.5}MnO_4$? Because our study is one to directly measure both the orbital and magnetic correlations, and their temperature dependences, it is difficult to be certain. However, there are intriguing results obtained by other resonant x-ray studies at the *K* edge of other 3*d* transition metal compounds that suggest that such effects may be a general feature of strongly correlated systems. In $LaMnO_3$ RXS studies[40] at the Mn *K* edge observed scattering at the symmetry forbidden (300) position. Such measurements, indirectly attributed to orbital ordering via Jahn-Teller distortions, showed that the intensity increases dramatically at T_{OO} and thereafter remained almost constant until just above T_N where the integrated intensity increased by 50%. In $KCuF_3$ a doubling of the integrated intensity of the orbital order reflection was observed upon cooling just above T_N.[41,42] What is surprising about all of these results is that the increase occurs well below the orbital ordering transition temperature where the orbital order parameter is expected to be saturated. A number of different causes of this effect have been proposed. Ishihara and Maekawa[43] suggested that such anomalous changes may signal a change in the type of orbital order. However, our energy resonance data do not show any dramatic changes in profile around T_N. Paolasini *et al.*[41] suggested that the magnetic order is driven by the orbital order and that the spin exchange constants are determined by the relative orientation of the occupied orbitals. Alternatively, Binggeli and Altarelli[44] have suggested that in $KCuF_3$ the increase in the orbital order reflection at T_N may simply suggest a low temperature structural transition. In $La_{0.5}Sr_{1.5}MnO_4$ our results suggest an interplay between magnetic and orbital order and/or Jahn-Teller distortions below T_N in the absence of any structural transitions. The origin of the temperature dependence of the orbital order signal, however, remains an unsolved problem.

V. CONCLUSIONS

We have presented the energy dependence of the scattered intensity at a fixed wave vector of $\vec{q}_{OO}=(\frac{1}{4},\frac{1}{4},0)$ and $\vec{q}_{AF}=(\frac{1}{4},-\frac{1}{4},\frac{1}{2})$ through the Mn L_3 and L_2 edges.

A good agreement was found between the experimental data and theoretical fits which included a realistic description of the spin direction. A single set of parameters describing the crystal field was used for both orbital and magnetic reflections. It is noted that there was a slight discrepancy in the branching ratio (L_3/L_2) between data and theoretical results.

The results of the fitting procedure demonstrate that the orbital ordering is predominantly of the $d_{x^2-z^2}/d_{y^2-z^2}$ type. A satisfactory fit to both data sets could not be obtained with the other proposed type of the orbital ordering $(d_{3x^2-r^2}/d_{3y^2-r^2})$. The inclusion of a small orthorhombic component of the crystal field, in the case of the $d_{x^2-z^2}/d_{y^2-z^2}$ type of the orbital ordering, moderately improved the fits. Such results are consistent with the x-ray linear dichroism results of Huang *et al.*[39] In addition, the x-ray scattering results confirm the existence of long-range order.

Further theoretical investigation of the orbital scattering indicates that the intensity of the L_3 edge is strongly sensitive to the Jahn-Teller distortion, whereas the L_2 edge is mostly sensitive to orbital order. We believe this is a general feature that can be used as a guideline in the interpretation of the orbital scattering in other manganite systems. We conclude, therefore, in the specific case of $La_{0.5}Sr_{1.5}MnO_4$ presented here, that the system is highly influenced by Jahn-Teller distortions.[44]

Measurements of the temperature dependence of the ratio of the integrated intensities at the L_3 and L_2 edges suggest that there is a strong coupling between the Jahn-Teller distortion and the long-range magnetic order. These results are not consistent with a change of the orbital order type at T_N, as previously suggested,[21] and the origin of the temperature dependence of the orbital order signal remains an open issue.

ACKNOWLEDGMENTS

This work was supported by the Synchrotron Radiation Related Theory Network, SRRTN, of the EU. S.B.W. would like to thank the European Commission for support in the frame of the "Training and Mobility of Researchers" pro-

gram. N.S. gratefully acknowledges the assistance of Paolo Carra in learning how to use the Cowan and "Racah" codes. P.D.H. would like to acknowledge support from the University of Durham Research Foundation. We are grateful for financial support from EPSRC for T.A.W.B., and to CLRC for access to the SRS and ESRF.

[1] I. S. Osborne, Science **288**, 461 (2000).
[2] P. G. Radaelli, D. E. Cox, M. Marezio, and S.-W. Cheong, Phys. Rev. B **55**, 3015 (1997).
[3] T. Mutou and H. Kontani, Phys. Rev. Lett. **83**, 3685 (1999).
[4] D. Khomskii and J. vandenBrink, Phys. Rev. Lett. **85**, 3329 (2000).
[5] T. Hotta, E. Dagotto, H. Koizumi, and Y. Takada, Phys. Rev. Lett. **86**, 2478 (2001).
[6] A. Daoud-Aladine, J. Rodriguez-Carvajal, L. Pinsard-Gaudart, M. T. Fernandez-Diaz, and A. Revcolevschi, Phys. Rev. Lett. **89**, 097205 (2002).
[7] Y. Moritomo, Y. Tomioka, A. Asamitsu, Y. Tokura, and Y. Matsui, Phys. Rev. B **51**, R3297 (1995).
[8] B. J. Sternlieb, J. P. Hill, U. C. Wildgruber, G. M. Luke, B. Nachumi, Y. Moritomo, and Y. Tokura, Phys. Rev. Lett. **76**, 2169 (1996).
[9] J. B. Goodenough, Phys. Rev. **100**, 564 (1955).
[10] J. Herrero-Martin, J. Garcia, G. Subias, J. Blasco, and M. C. Sánchez, cond-mat/0406407 [Phys. Rev. B (to be published)]
[11] V. Ferrari, M. Towler, and P. B. Littlewood, Phys. Rev. Lett. **91**, 227202 (2003).
[12] E. O. Wohlan and W. C. Koehler, Phys. Rev. **100**, 545 (1955).
[13] Y. Murakami, H. Kawada, H. Kawata, M. Tanaka, T. Arima, Y. Moritomo, and Y. Tokura, Phys. Rev. Lett. **80**, 1932 (1998).
[14] S. Ishihara and S. Maekawa, Rep. Prog. Phys. **65**, 561 (2002).
[15] T. Mizokawa and A. Fujimori, Phys. Rev. B **56**, R493 (1997).
[16] I. S. Elfimov, V. I. Anisimov, and G. A. Sawatzky, Phys. Rev. Lett. **82**, 4264 (1999).
[17] M. Benfatto, Y. Joly, and C. R. Natoli, Phys. Rev. Lett. **83**, 636 (1999).
[18] I. V. Solovyev and K. Terakura, Phys. Rev. Lett. **83**, 2825 (1999).
[19] P. Mahadevan, K. Terakura, and D. D. Sarma, Phys. Rev. Lett. **87**, 066404 (2001).
[20] P. Benedetti, J. vandenBrink, E. Pavarini, A. Vigliante, and P. Wochner, Phys. Rev. B **63**, 060408(R) (2001).
[21] S. Ishihara and S. Maekawa, Phys. Rev. Lett. **80**, 3799 (1998).
[22] H. Ohsumi, Y. Murakami, T. Kiyama, H. Nakao, M. Kubota, Y. Wakabayashi, Y. Konishi, M. Izumi, M. Kawasaki, and Y. Tokura, J. Phys. Soc. Jpn. **72**, 1006 (2003).
[23] S. B. Wilkins, P. D. Hatton, M. D. Roper, D. Prabhakaran, and A. T. Boothroyd, Phys. Rev. Lett. **90**, 187201 (2003).
[24] S. B. Wilkins, P. D. Spencer, P. D. Hatton, S. P. Collins, M. D. Roper, D. Prabhakaran, and A. T. Boothroyd, Phys. Rev. Lett. **91**, 167205 (2003).
[25] C. W. M. Castleton and M. Altarelli, Phys. Rev. B **62**, 1033 (2000).
[26] S. S. Dhesi, A. Mirone, C. Nadai, P. Ohresser, P. Bencok, N. B. Brookes, P. Reutler, A. Revcolevschi, A. Tagliaferri, O. Toulemonde, and G. vanderLaan, Phys. Rev. Lett. **92**, 056403 (2004).
[27] K. J. Thomas, J. P. Hill, S. Grenier, Y.-J. Kim, P. Abbamonte, L. Venema, A. Rusydi, Y. Tomioka, Y. Tokura, D. F. McMorrow, G. Sawatzky, and M. van Veenendaal, Phys. Rev. Lett. **92**, 237204 (2004).
[28] R. D. Cowan, J. Opt. Soc. Am. **58**, 808 (1968).
[29] R. D. Cowan, *The Theory of Atomic Structure and Spectra* (University of California, Berkeley, 1981).
[30] G. van der Laan and B. T. Thole, Phys. Rev. B **43**, 13 401 (1991).
[31] P. H. Butler, *Point Group Symmetry Applications* (Plenum, New York, 1981).
[32] There is experimental indication for the spin direction in the [210]-direction (Ref. 8), but in our latest theoretical study (Ref. 35), we estimate it to be [110] or very close to it.
[33] A. Thomson, D. Vaughan, E. Gullikson, M. Howells, K.-J. Kim, J. Kirz, J. Kortright, I. Lindau, P. Pianetta, A. Robinson *et al.*, *X-Ray Data Booklet* (Lawrence Berkeley National Laboratory, University of California, Berkeley, CA 94720, 2001).
[34] P. Carra and B. T. Thole, Rev. Mod. Phys. **66**, 1509 (1994).
[35] N. Stojić, N. Binggeli, and M. Altarelli (unpublished).
[36] J. P. Hannon, G. T. Trammell, M. Blume, and D. Gibbs, Phys. Rev. Lett. **61**, 1245 (1988).
[37] F. de Groot, Coord. Chem. Rev. **249**, 31 (2005).
[38] S. Grenier, J. P. Hill, D. Gibbs, K. J. Thomas, M. v. Zimmermann, C. S. Nelson, V. Kiryukhin, Y. Tokura, Y. Tomioka, D. Casa, T. Gog, and C. Venkataraman, Phys. Rev. B **69**, 134419 (2004).
[39] D. J. Huang, W. B. Wu, G. Y. Guo, H.-J. Lin, T. Y. Hou, C. F. Chang, C. T. Chen, A. Fujimori, T. Kimura, H. B. Huang, A. Tanaka, and T. Jo, Phys. Rev. Lett. **92**, 087202 (2004).
[40] Y. Murakami, J. P. Hill, D. Gibbs, M. Blume, I. Koyama, M. Tanaka, H. Kawata, T. Arima, Y. Tokura, K. Hirota, and Y. Endoh, Phys. Rev. Lett. **81**, 582 (1998).
[41] L. Paolasini, R. Caciuffo, A. Sollier, P. Ghigna, and M. Altarelli, Phys. Rev. Lett. **88**, 106403 (2002).
[42] R. Caciuffo, L. Paolasini, A. Sollier, P. Ghigna, E. Pavarini, J. vandenBrink, and M. Altarelli, Phys. Rev. B **65**, 174425 (2002).
[43] S. Ishihara and S. Maekawa, Phys. Rev. B **62**, R9252 (2000).
[44] N. Binggeli and M. Altarelli, Phys. Rev. B **70**, 085117 (2004).